*J Mater Sci: Mater Electron* (2021) 32:4146–4156

# Influence of thiourea in the precursor solution on the structural, optical and electrical properties of CZTS thin films deposited via spray coating technique

P. Prabeesh[1], V. G. Sajeesh[1], I. Packia Selvam[1], and S. N. Potty[1,*]

[1] *Centre for Materials for Electronics Technology (C-MET), Scientific Society, Ministry of Electronics & Information Technology, Government of India, Shoranur Road, Athani P.O, Thrissur 680 581, India*

**Received:** 12 August 2020
**Accepted:** 21 December 2020
**Published online:** 8 January 2021



## ABSTRACT

CZTS films were prepared by spray coating using non-aqueous precursor solutions with and without sulphur source and studied their structural, optical and electrical properties. The films prepared by both the routes were sulphurized at different temperatures to study the effect of temperature on the phase formation. Phase purity was confirmed by XRD, Raman analysis and Rietveld refinement technique. The studies revealed proper phase and crystallinity for the films of both routes sulphurized at 550 °C. These films exhibited dense and improved grain structure, optimal bandgap and higher absorption coefficient. The non-thiourea films sulphurized at 550 °C had a carrier concentration of $1.544 \times 10^{19}$ $cm^{-3}$, mobility of 0.87 $cm^2V^{-1}$ $s^{-1}$ and resistivity of 0.46 Ω·cm, while the thiourea films achieved carrier concentration, mobility and resistivity of $3.67 \times 10^{19}$ $cm^{-3}$, 0.33 $cm^2V^{-1}$ $s^{-1}$ and 0.52 Ω·cm, respectively. The comparative study demonstrates that the films under investigation have the potential for the fabrication of efficient solar cells.

## 1 Introduction

Chalcogenide-based CZTS thin-film solar cells have undergone remarkable developments over the past few decades [1]. Because of its excellent photovoltaic properties, investigations are being carried out by various groups to establish an ideal fabrication method for phase pure CZTS film. The highest conversion efficiency reported for CZTSSe solar cells is 12.6%, which is processed through a solution-based route [2]. Several non-vacuum techniques were already reported in the literature [3–7]. Various approaches were adopted in these routes by changing parameters such as composition ratio, type of annealing atmosphere, type of precursor solution [3, 6], precursor layer thickness [8], annealing/sulphurization temperature [4]. Among the non-vacuum routes, spray coating is cost-effective and suitable for

Address correspondence to E-mail: snpotty@cmet.gov.in


https://doi.org/10.1007/s10854-020-05156-y

high volume manufacturing. The advantages of spray coating are high deposition rate and reproducibility; high-quality targets or vacuum are not needed here. With the spray coating technique, the highest power conversion efficiency reported for CZTS is only 8.1% [9]. Water is used as a solvent in the spray coating process in most of the already published reports. The dependence of the solvent type on the final properties of CZTS films is also reported [10]. The lower efficiency of the spray-coated CZTS is mainly due to the lack of proper understanding of the material formation. Many researchers already studied different spray coating parameter, such as the effect of solvent, substrate temperature, deposition time, precursor composition, spray volume [9, 11–17]. With a digital literature survey available up to date, no report on spray coating has been reported so far using a non-thiourea precursor in a non-aqueous coating solution, and there is no comparative study on the influence of thiourea in an organic solvent-based coating solution. Organic solvents were generally used to increase the solubility of the precursors [18]. 2-methoxy ethanol has been used as a solvent with monoethanolamine (MEA) as a stabilizing agent in most of the solution-based techniques such as spin and dip coatings. The films obtained in this route exhibited optimum properties for CZTS thin films [4, 19]. MEA has optimum viscosity and boiling point (125 °C) and can solubilize a variety of different precursors. Tanaka et al. [20] fabricated the best-quality CZTS thin film by spin coating of non-thiourea precursor solution followed by sulphurization. Keeping this in mind, CZTS thin films were prepared in this study by spray coating using an organic solvent with two types of precursor solutions and studied the effect of sulfurization temperature on the properties of CZTS thin films. Sulphurizations were conducted in (95%) $N_2$ + (5%) $H_2S$ atmosphere, which would reduce the possible sulphur loss during the annealing process or to incorporate sulphur into the lattice. This work presents a comparison of CZTS films prepared with and without thiourea in the coating solution and the investigation of how the inclusion of sulphur source (thiourea) will influence the structural, surface morphological, optical and electrical properties of the film.

## 2 Experimental techniques

For preparing a coating solution, acetates and chlorides were used as raw materials, because these compounds are cheap and readily available from commercial suppliers. Metal acetates have low sensitivity to moisture [21]. The chemicals were purchased from Merck and used without further purification. Precursor solution without thiourea was made by dissolving copper (II) acetate monohydrate (0.02 M), zinc (II) acetate dihydrate (0.01 M), tin (II) chloride (0.01 M) into 200 mL 2-methoxy ethanol (labelled as Sol I). On the other hand, a precursor solution with thiourea was made by adding 0.08 M thiourea into Sol I (labelled as Sol II). Substrate cleaning is an important step in the thin film fabrication; the substrates for deposition were cleaned ultrasonically with soap solution, acetone, ethanol and distilled water for 15 min each in succession. The substrates were rinsed with distilled water in between each step. The films were finally dried in the free flow of nitrogen gas and kept in desiccators.

Films were coated by spraying precursor solution on to the pre-cleaned substrates at a flow rate of 8 mL/min using a custom fabricated spray coating set up. The substrate temperature was kept at 300 °C throughout the process. Airblast atomizer containing pure nitrogen gas with flow rate 4 L/min was used for spraying. The distance between spray nozzle and substrate was 10 cm. Figure 1 shows the schematic diagram of the spray coating system used in this work. After coating, the films were further sulphurized to achieve complete phase formation and also to improve crystallite properties. The sulphurization has been carried out in a controlled ($N_2$(95%) + $H_2S$(5%)) atmosphere at various temperatures to study the effect of sulphurization on optoelectronic properties. The substrate was held at 300 °C during the deposition; however, thiourea tends to form organic by-products that may present in the film at this temperature [22]. As-deposited films may be sulphur-deficient (for TU system) or sulphur-free (for NTU system). Hence annealing of the films at a higher temperature in a controlled reactive atmosphere is necessary for obtaining the desired stoichiometry and the required material properties [23]. For this, films were kept in a tubular furnace (Lenton Make) and the temperature was increased from room temperature to the desired temperature at a rate of 5 °C per minute. The

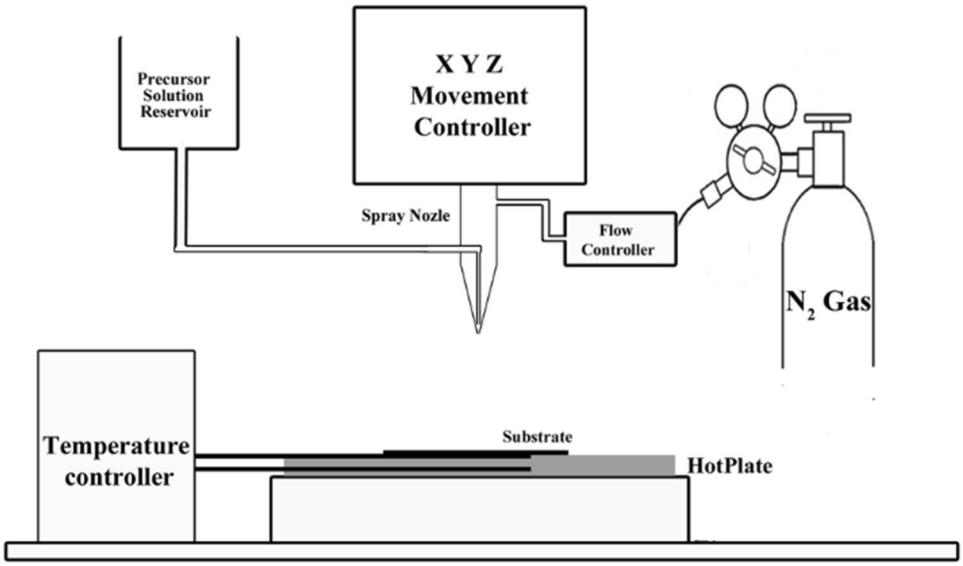


**Fig. 1** Schematic diagram of spray coating system used in the study

temperature was kept constant for 30 min when it reached maximum temperature and thereafter allowed to cool to room temperature. For convenience, the precursor films coated were coded as NTU (samples prepared using Sol I) and TU (samples prepared using Sol II); temperature is added to these codes to indicate the temperature at which the sulphurization has been done.

Crystal structure and phase purity of the films were investigated by X-ray diffraction (Bruker AXS D8 advanced and Rigaku Miniflex 600) and Raman spectroscopy with 532 nm laser irradiation (Thermoscientific-DXR). Structural properties were further investigated by the Rietveld refinement technique using the General Structure Analysis System (GSAS) software [24]. For structural refinement, high resolution grazing incidence X-ray diffraction (GI-XRD) data were recorded with a step size of 0.02° and a collection time of 3 s per step, at 1° grazing angle. The surface morphology of the films was investigated by scanning electron microscopy (SEM) (Zeiss Evo 18 Research), field emission SEM (FESEM) (FEI NOVO NANOSEM-450). Elemental composition, optical properties (bandgap and absorption coefficient) and electrical properties (carrier concentration, mobility and resistivity) were determined by Energy Dispersive X-ray Spectroscopy (EDXS) attached with SEM, UV–visible spectroscopy (Perkin Elmer Lambda 35) and Hall Effect measurement system (Ecopia HMS 3000 with 0.54 T permanent magnetic field), respectively.

## 3 Results and discussion

Figure 2a and b show the XRD patterns of the CZTS films coated with Sol-I and Sol-II respectively that have been sulphurized at different temperatures from 450 to 600 °C. All films showed characteristic peaks of CZTS and the peaks were identified with the help of ICDD powder diffraction file 26-0575. The film NTU450 exhibited a few other peaks in addition to those of CZTS. These peaks were identified as due to $SnS_2$, (ICDD file 89-2028). Similarly, additional XRD peaks were observed in the film NTU500 also; these were due to $Cu_2SnS_3$ phase (ICDD file 27-0198). In addition, the film NTU600 exhibited extra peaks due to the secondary phases, $SnS_2$ and $Cu_4SnS_4$ (ICDD file for $Cu_4SnS_4$—27-0196). As seen in the figure, the XRD patterns of the films NTU550 and TU550 sulphurized at 550 °C contain only the peaks of CZTS and thus are phase pure. These films did not show any other phases even at higher sulphurizing temperatures. As seen in the XRD patterns, the number of peaks and peak intensity of these films increase with sulphurizing temperature. Thus, the crystallinity of the films was found to increase with an increase in sulphurization temperature from 400 to 600 °C.

$Cu_2ZnSnS_4$ possesses a tetragonal structure and the lattice constants were calculated based on this symmetry from the XRD patterns (Table 1). These values are in good agreement with the single crystal data, $a = b = 0.5427$ nm and $c = 1.0848$ nm (ICDD-PDF No.26-0575). No appreciable difference in the lattice

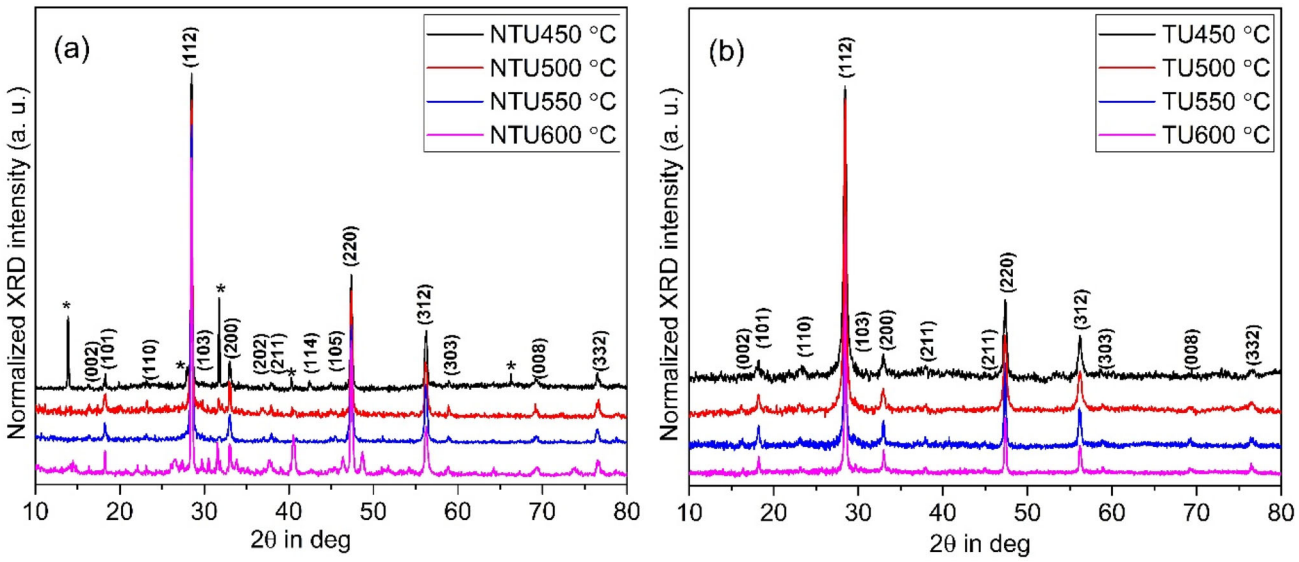


**Fig. 2** XRD patterns of CZTS films prepared with **a** sol-I and **b** sol-II and sulphurized at different temperatures

constants of CZTS has been detected in the samples with increase in sulphurization temperature, and even with the additional phases. Change in crystalline size with sulphurizing temperatures was studied using Scherrer's formula and W–H relation and the results are given in Table 1. The average crystallite size of the CZTS films prepared by the two routes was found to increase with sulphurizing temperature. In both cases, the larger crystallite size was observed for the films sulphurized at 600 °C, and the size obtained through the Scherrer formula was smaller than that of the W–H method. As seen in the table, the average crystallite size increases with an increase in sulphurization temperature. The higher crystallite size was observed for both NTU600 and TU600 films; however, the X-ray diffraction analysis revealed secondary/ ternary phases in these films at this sulphurization temperature. The average size of the crystallites in film NTU550 and TU550 was found to be 52 nm and 59 nm respectively by Scherer analysis, whereas the same was 56 nm and 60 nm by W–H relation. A higher crystalline size was observed for the thiourea system compared to the non-thiourea system. Lattice strain on the films was calculated using W–H relation and the values are given in Table 1. A higher strain was observed for the film NTU600.

ZnS, $Cu_2ZnS_3$, $Cu_4ZnSnS_4$ are the major secondary/ternary phases commonly observed in the preparation of CZTS [25]. X-ray diffraction peaks of these phases coincide with those of the CZTS, and hence it is difficult to confirm the phase purity from XRD alone. The phase purity of the CZTS films was

**Table 1** Lattice parameters and crystallite size of CZTS films prepared with (a) sol-I and (b) sol-II and sulphurized at different temperatures

| Sample Name | Lattice parameter | | Scherrer | W–H relation | |
|---|---|---|---|---|---|
| | $a = b$ (Å) | $c$ (Å) | Crystallite size *(nm)* | Crystallite size (nm) | Strain |
| NTU450 | 5.423 | 10.817 | 42 | 43 | 0.0007 |
| TU450 | 5.427 | 10.887 | 38 | 39 | 0.0087 |
| NTU500 | 5.440 | 10.823 | 46 | 50 | 0.0043 |
| TU500 | 5.426 | 10.911 | 47 | 51 | 0.0023 |
| NTU550 | 5.424 | 10.821 | 52 | 56 | 0.0012 |
| TU550 | 5.428 | 10.882 | 59 | 60 | 0.0008 |
| NTU600 | 5.433 | 10.785 | 56 | 62 | 0.0342 |
| TU600 | 5.424 | 10.744 | 70 | 69 | 0.0021 |
| ICDD | 5.4270 | 10.8480 | – | – | – |

further investigated by Raman spectroscopy and the spectra are shown in Fig. 3.

As shown in Fig. 2a and b, the films possess characteristic Raman vibrational modes of CZTS at 249/250 $cm^{-1}$, 328–334 $cm^{-1}$, 285/286 $cm^{-1}$, 351/352 $cm^{-1}$ and 366/374 $cm^{-1}$ irrespective of the sulphurization temperature. Peaks at 249/250 $cm^{-1}$, 328–332 $cm^{-1}$, 285/286 $cm^{-1}$, 351/352 $cm^{-1}$ and 366/374 $cm^{-1}$ correspond to the B(LO), A, A, B(TO) and B(LO) vibrational modes of kesterite phase, respectively [3, 25, 26]. Raman spectra of film NTU450 consist of a few additional peaks at 275 $cm^{-1}$, 291 $cm^{-1}$ and 316 $cm^{-1}$ in addition to the kesterite vibrational modes. These peaks are identified as the vibrational modes of ZnS [25, 27], $Cu_2SnS_3$ [25], and $SnS_2/Cu_3SnS_4$, respectively [27–30]. The origin of the mode at 317 $cm^{-1}$ is not clear since this is coinciding with the major modes of $SnS_2$ and $Cu_3SnS_4$ [27, 31]. XRD analysis revealed the presence of $SnS_2$ phase in the film NTU450. Films TU400 and TU450 showed another peak at 274 $cm^{-1}$, which is due to ZnS phase [25, 26]. This secondary phase was not observed in the XRD analysis. Raman spectra of film NTU500 exhibited vibrational modes at 291 $cm^{-1}$ and 316 $cm^{-1}$ corresponding to impurity phases $Cu_2SnS_3$ and $SnS_2/Cu_3SnS_4$, respectively [28, 30]. The film NTU600 showed peaks at 304 $cm^{-1}$ and 316 $cm^{-1}$ corresponding to secondary phases $Sn_2S_3$ and $SnS_2/Cu_3SnS_4$, respectively [5, 28, 29, 31]. In addition to the peaks at 249 $cm^{-1}$, 334 $cm^{-1}$ and 366 $cm^{-1}$, Raman spectra of the films NTU500 and NTU550 showed peaks at 284 $cm^{-1}$ and 352 $cm^{-1}$. Among the peaks, those at 284 $cm^{-1}$ and 334 $cm^{-1}$ correspond to the A vibrational mode, whereas peaks at 249 $cm^{-1}$, 352 $cm^{-1}$ and 366 $cm^{-1}$ correspond to the B(TO LO) vibrational mode of CZTS phase [26]. When sulphurization temperature was increased to 600 °C (TU600), a peak at 160 $cm^{-1}$ of SnS and another peak at 287 $cm^{-1}$ of $Cu_2SnS_3$ were observed along with the peaks of CZTS [25]. Thus, Raman studies confirmed the formation of phase pure CZTS in the films NTU550, TU500 and TU550. For photovoltaic devices, crystallinity of the film is also important [32]. Here, the films NTU600 and TU600 exhibited higher crystallinity, but contains secondary phases. Thus the films NTU550 and TU550 possess phase purity and better crystallinity (Table 1).

In addition to the phase formation and identification, investigations such as lattice and bond angle distortion are also important in the structural characterization of CZTS thin films. To carry out structural refinement by Rietveld analysis, high-quality data were obtained from high resolution grazing incidence X-ray diffraction. EXPGUI, the graphical interface of GSAS software, was used for the refinement process [33]. Tetragonal kesterite type model ($a = b = 5.427$ Å, $c = 10.871$ Å, $\alpha = \beta = \gamma = 90°$) in the S.G 14 (S.G No: 82) was the starting model [24, 34]. Figure 4 shows the rietveld refined plots of films sulphurized at 550 °C of both NTU and TU. The agreement factors of the fit for NTU550 are Wrp = 0.2030, $Rf^2 = 0.1448$ and $\chi^2 = 1.287$ and for TU550

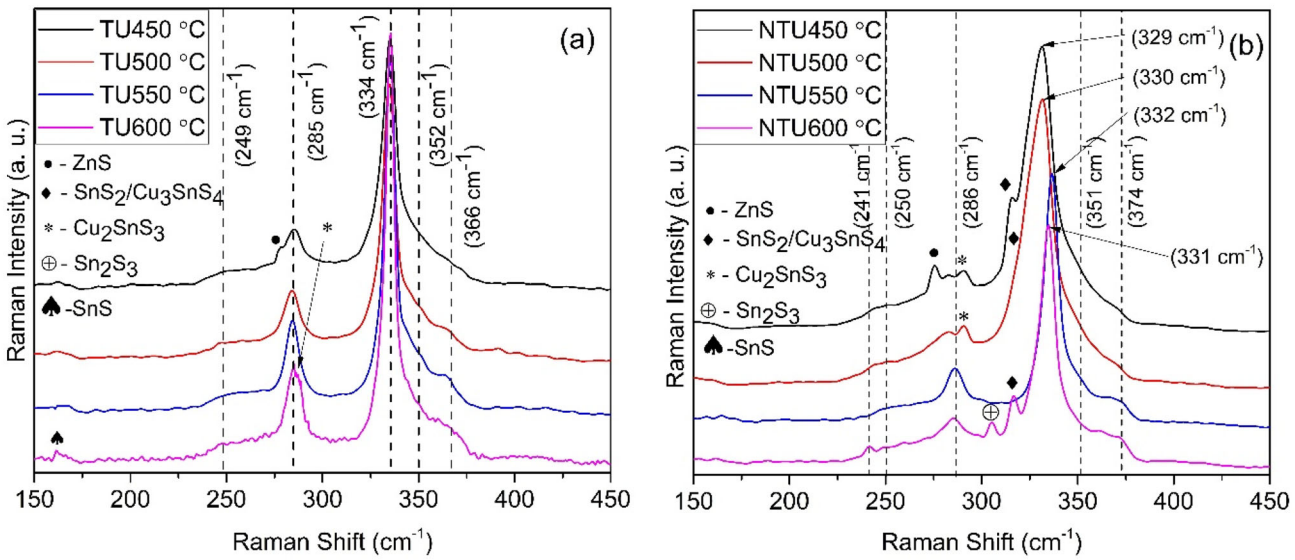


**Fig. 3** Raman spectra of CZTS films prepared with **a** sol-I and **b** sol-II and sulphurized at different temperatures

are Wrp = 0.2789, $R_f^2$ = 0.2592 and $\chi^2$ = 1.260. The lattice parameters $a = b$ and $c$ of films were extracted from the refined data. Refined lattice parameters for NTU550 were $a = b$ = 5.4309465 Å, $c$ = 10.858355 Å and $c/2a$ = 0.9993 and for TU550 are $a = b$ = 5.4307 Å, $c$ = 10.8294 Å and $c/2a$ = 0.9971 which is close to the reported values of lattice constants for kesterite mineral data ($a = b$ = 5.428(2) Å, $c$ = 10.864(4) Å and $c/2a$ = 0.9854(5)) [34–36]; however, a minor distortion in c axis has been observed in both the cases.

In the case of kesterite-type crystals, tetrahedral distortion can be expressed in terms of cation–anion–cation bond angles (ideal value is 109.47°). However, in the kesterite crystal structure, the Cu–S–Sn and Zn–S–Sn angles are smaller, and Cu–S–Zn and Cu–S–Cu angles are larger than this ideal value. In this study, for NTU550, the bond angles obtained were 107.317(6)° for Cu–S–Sn, 108.21(10)° for Zn–S–Sn, 111.321(11)° for Cu–S–Zn and 110.510(9)° for Cu–S–Cu. In the case of TU550, the bond angles were 108.528(14)° for Cu–S–Sn, 109.33(7)° for Zn–S–Sn, 112.257(7)° for Cu–S–Zn and 109.612(7)° for Cu–S–Cu. The bond angles determined are in good agreement with that of the kesterite structure [34, 35, 37]. Comparing the two systems, the TU films show higher bond angles except for the Cu–S–Cu angle, which may be due to the induced strain, as seen in Table 1 [24].

Elemental compositions of the films were investigated by EDXS are given in Table 2. For CZTS, ideal stoichiometry is when Cu/(Zn + Sn) and Zn/Sn ratios are unity. However, it has been reported that non-stoichiometry in CZTS is favourable for obtaining higher efficiency [2]. p-type conductivity in CZTS is attributed to $Cu_{Zn}$ antisite and Cu vacancy; however, compared to the vacancy, the antisite has a deeper accepter level [38]. Most of the experimental results already reported indicate Cu-poor and Zn-rich conditions for achieving better efficiency in CZTS cells [18, 30, 39, 40]. Researchers have been working with various deposition routes to control defect engineering without secondary phase formation. Studies on elemental composition ratios provide information about the Cu-poor and Zn-rich nature of the films.

As seen in the table, the stoichiometry has considerably deviated for the film NTU450. This indicates that CZTS phase formation is not completed when sulphurized at 450 °C. The sulphur concentration of NTU decreases with an increase in sulphurization temperature to 550 °C. In this work, the composition ratios of the spray-coated films were Cu/(Zn + Sn) = 0.91 and Zn/Sn = 0.92 for the film NTU550; the required zinc-rich condition has been not obtained here. Huang et.al. reported similar stoichiometric variations for spray-coated CZTS films [41]. A higher variation in stoichiometry was observed for the film TU450. The Cu/(Zn + Sn) and Zn/Sn ratios of the film TU550 were 0.97 and 0.99, respectively. As seen in the table, the film TU550 is Cu poor. However, the

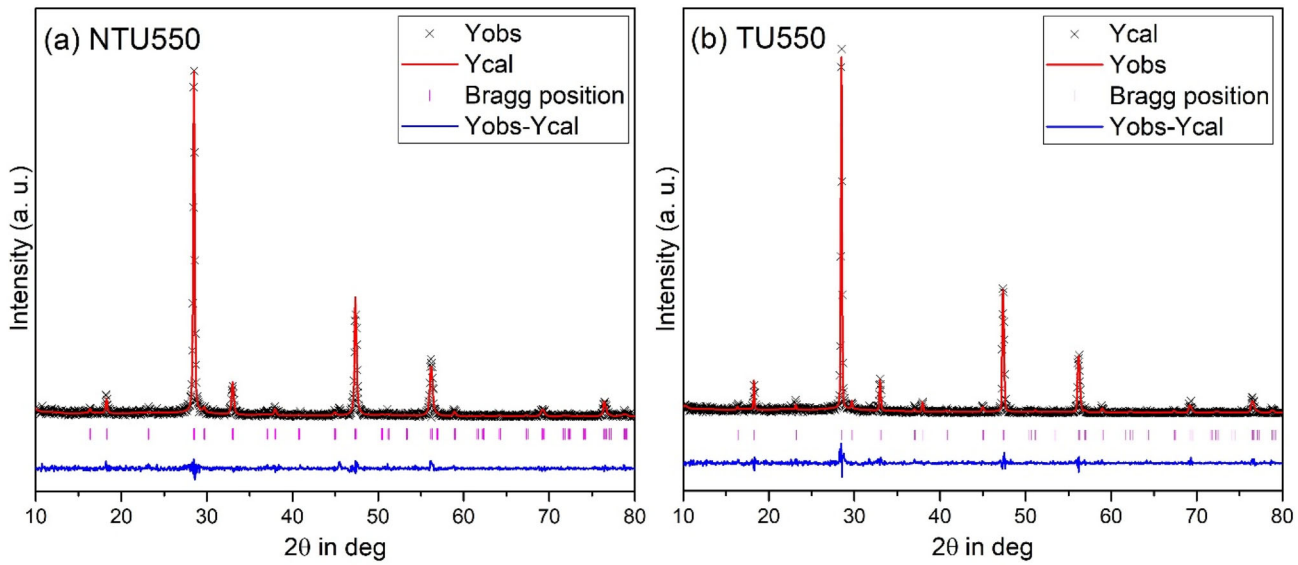


**Fig. 4** Rietveld refinement plot of **a** NTU550 and **b** TU550; Black dots represent experimental data, red line is the calculated fit, pink vertical lines are the positions of refined phase reflections and blue line is the difference line between the experimental and fitted data

**Table 2** EDXS results of CZTS films coated with Sol-I and Sol-II and sulphurized at different temperatures

| Sample name | EDXS results | | | | | |
|---|---|---|---|---|---|---|
| | Cu (at%) | Zn (at%) | Sn (at%) | S (at%) | Cu/(Zn + Sn) | Zn/Sn |
| NTU450 | 14.49(± 4) | 9.01 (± 5) | 17.17 (± 2) | 59.33 (± 4) | 0.55 | 0.52 |
| TU450 | 22.87(± 6) | 11.75(± 3) | 10.83(± 3) | 54.55(± 6) | 1.01 | 1.08 |
| NTU500 | 20.88 (± 5) | 10.83(± 3) | 10.79 (± 4) | 57.55 (± 6) | 0.97 | 1.00 |
| TU500 | 23.0 (± 4) | 11.7 (± 4) | 11.8 (± 3) | 53.5 (± 4) | 0.98 | 0.99 |
| NTU550 | 23.64 (± 4) | 12.38(± 5) | 13.39 (± 2) | 50.59 (± 5) | 0.91 | 0.92 |
| TU550 | 22.78(± 4) | 11.67(± 5) | 11.8 (± 4) | 53.75(± 3) | 0.97 | 0.99 |
| NTU600 | 23.29 (± 4) | 12.23(± 5) | 10.05 (± 4) | 54.43 (± 5) | 1.05 | 1.22 |
| TU600 | 26.39(± 2) | 11.31(± 4) | 13.05(± 2) | 49.25(± 8) | 1.08 | 0.87 |

Zn/Sn ratio was found to decrease with an increase in sulphurization temperature. Sn loss is reported in CZTS with annealing temperature [42]; on the other hand, Sn content was found to increase with an increase in sulphurization temperature. The results shown in Table 2 reveal non-stoichiometry in all the films that have been sulphurized at various temperatures.

Surface morphology and film thickness of spray-coated films were analysed by scanning electron microscopy and the images are shown in Fig. 5. As seen in the figures, the grain sizes increase with sulphurization temperature, which may be due to Ostwald ripening of grains at higher temperature [43]. Figure 5a–h shows the SEM images of films NTU450, TU450, NTU500, TU500, NTU550, TU550, NTU600 and TU600. As seen, cracks were observed in the films NTU450, TU500, NTU600 and TU600. The grain size is very small for the films prepared using Sol-II. Dense surface morphology with large grains was observed for the films NTU500, NTU550 and TU550. However, grains with different sizes and shapes were observed for NTU600 and TU600 films. The XRD and Raman studies revealed secondary and ternary phases in the films NTU600 and TU600; higher temperature sulphurization may lead to decomposition of CZTS and form secondary or ternary phases [44]. However, XRD and Raman investigations confirmed the phase purity of the films NTU550 and TU550. Grain and grain boundaries are clearly visible at this temperature. Thus, dense CZTS films with good microstructure were formed in both cases at the sulphurization temperature of 550 °C. The cross-sections of the films sulphurized at 550 °C are shown in Fig. 2i and j. The thicknesses of the films estimated were ~ 1.9 μm for NTU550 and 2.02 μm for TU550.

Figure 6 shows the $(\alpha h\upsilon)^2$ versus hυ plots of CZTS films sulphurized at various temperatures. Tauc's relation was used for estimating the bandgap of the film [4, 19]. The bandgap of the films was found to decrease from 1.53 to 1.33 eV for NTU system and 1.83 eV to 1.38 eV for TU system with an increase in sulphurization temperature. The observed change in bandgap may due to the increase in crystallite size and the presence of secondary phases [45–47]. Ansari et al. reported the influences of strain and crystallite size on the bandgap of CZTS films, and observed a decrease in bandgap with increase in crystallite size and decrease in the strain of the films [11]. The higher bandgap of films NTU450 and TU450 may due to the difference in crystallinity and the presence of secondary phases ZnS/SnS identified in Raman analysis [8, 32, 45]. When sulphurization temperature is increased, ZnS/SnS react with other metallic sulphides and form CZTS phase [26]. The bandgap was found to be 1.47 eV for NTU550 and ~ 1.49 eV for TU550. These values are close to the optimum value of 1.5 eV for single-junction solar cells. For both NTU and TU systems, the increase in sulphurization temperature from 550 to 600 °C decreases the bandgap.

Figure 7 shows the absorption coefficient versus wavelength plot for the films sulphurized at 550 °C. As shown, the films exhibit average absorption coefficients of ~ $8 \times 10^4$ $cm^{-1}$ and ~ $15 \times 10^4$ $cm^{-1}$ for the films NTU550 and TU550, respectively in the visible region. Thiourea films sulphurized at 550 °C showed a higher absorption coefficient than that of the non-thiourea system. The higher absorption coefficient indicates that a thin film with thickness ~ 2 μm fabricated in this study can absorb most of the incident photons.

The electrical properties of the films were measured at room temperature by a Hall effect

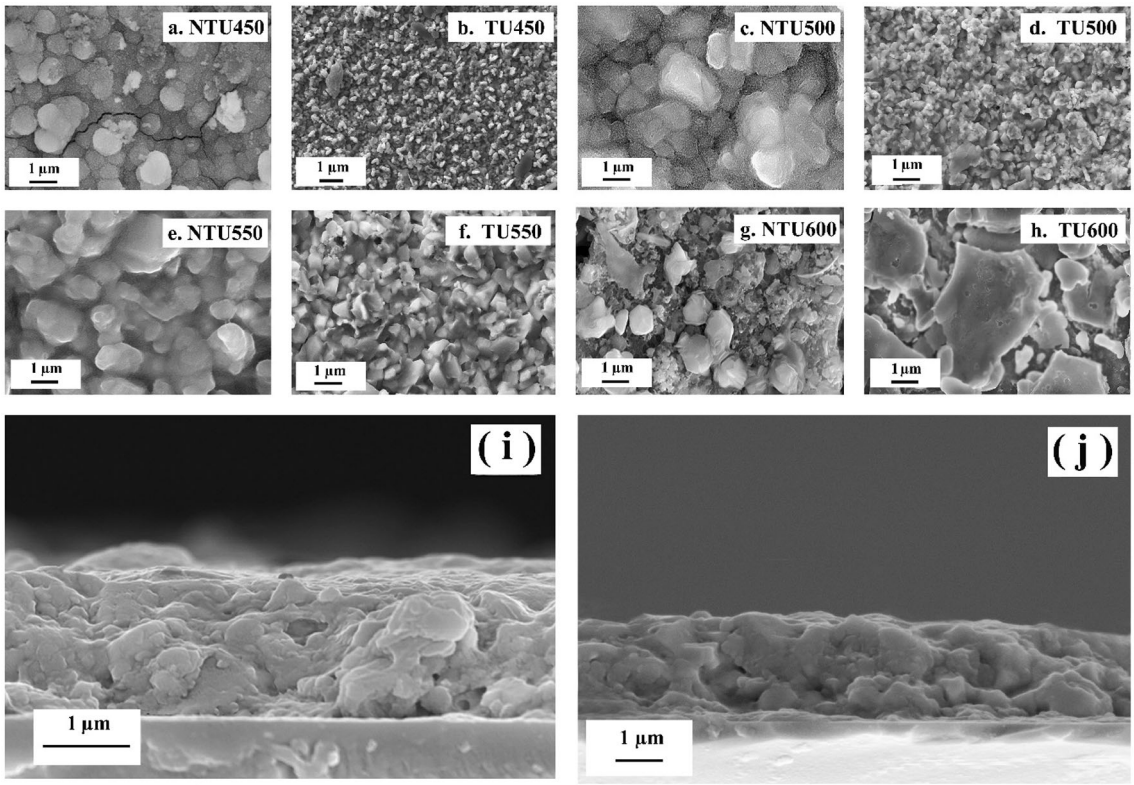


**Fig. 5** SEM images of CZTS films prepared with Sol-I and Sol-II and sulphurized at different temperatures (**a**-**h**) and cross-sectional images of (**i**) NTU500 and (**j**) TU500 for thickness measurement

measurement system with van der paw configuration having a permanent magnetic field intensity of 0.54 T. The positive sign of the Hall coefficient confirmed the *p*-type nature of conductivity. Carrier concentration, mobility and resistivity of the film NTU550 were $1.544 \times 10^{19}$ $cm^{-1}$ and 0.87 $cm^2V^{-1}S^{-1}$, 0.46 Ω·cm, while for the film TU550, the same were $3.67 \times 10^{19}$ $cm^{-1}$, 0.33 $cm^2V^{-1}S^{-1}$ and 0.52 Ω·cm, respectively. Compared to the film NTU550, the corresponding TU film exhibited slightly higher carrier concentration, but with lower mobility. The microstructure of the TU film revealed a lower grain size, and this may be the reason for the lower mobility. Similar results were published by Rajeshmon et al. [3] for CZTS films coated by spray coating using chloride precursor solution and water as a solvent. According to Long et al., the optimum values for resistivity, mobility and carrier concentration for CZTS films are 10 to $10^3$ Ω·cm, $10^{16}$ to $10^{18}$ $cm^{-3}$ and 1 to 10 $cm^2$/Vs, respectively [48]. However, several articles were published later with different electrical properties for CZTS films, fabricated by various techniques. Most of these articles reported lower resistivity, higher mobility and moderate carrier concentration for CZTS films [28, 49, 50].

## 4 Conclusion

Two different non-aqueous solutions, with and without sulphur source, were used to prepare CZTS films by spray coating and subsequent sulphur annealing. XRD and Raman spectroscopic investigations were used to study the structural properties of the films sulphurized at different temperatures. These studies revealed phase pure nature for the spray-coated films of both routes sulphurized at 550 °C. Secondary or ternary phases were observed in the films treated at lower or higher sulphurization temperatures. In both cases, the crystallite size of the films were increased with increase in sulphurization temperature. The structural properties of the 550 °C sulphurized films were further investigated by the Rietveld refinement technique. Refined lattice parameters are close to the reported lattice parameter for kesterite mineral. The changes in the bond angle

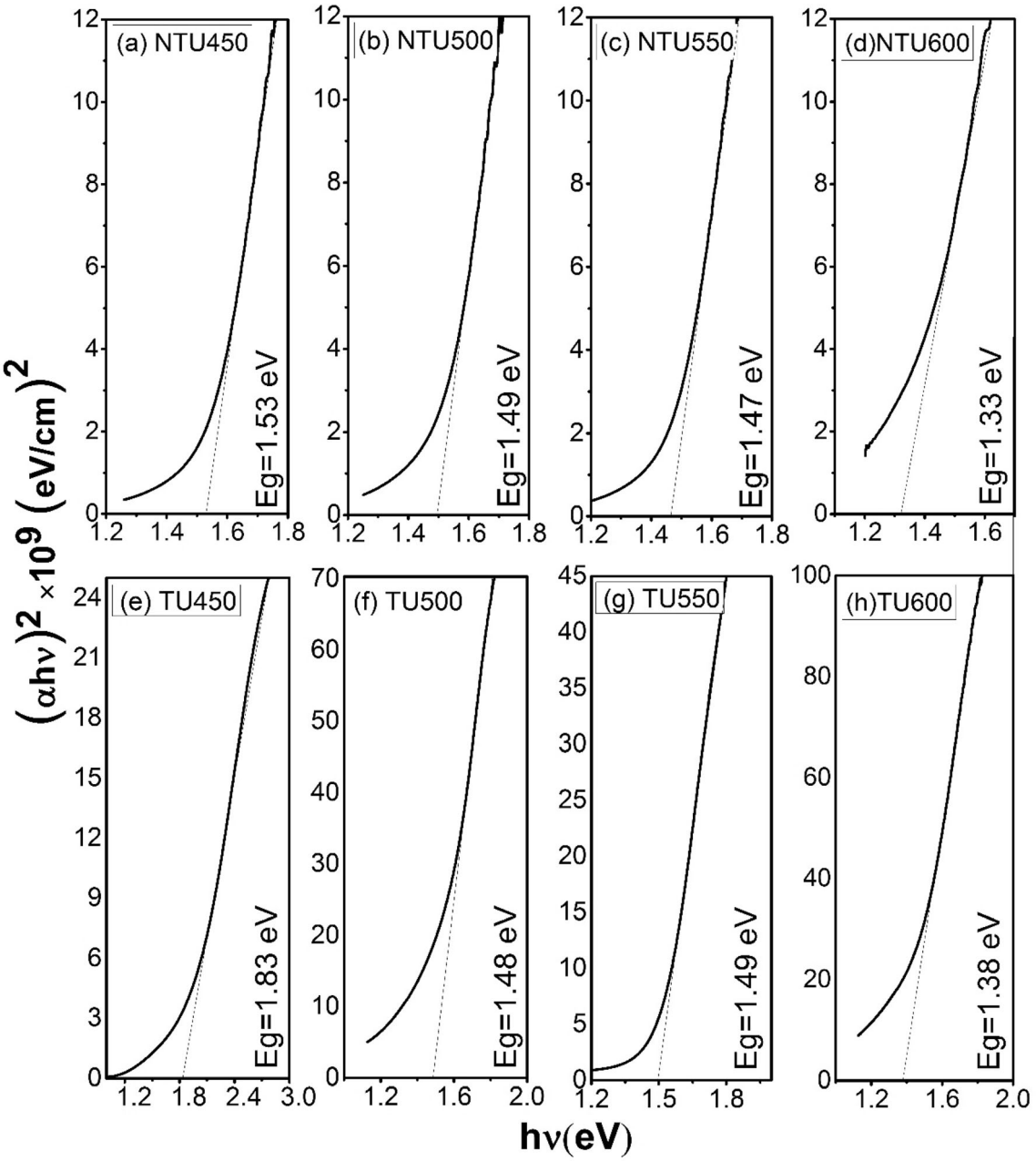


**Fig. 6** $(\alpha h\upsilon)^2$ versus $h\upsilon$ plots of CZTS films prepared with Sol-I and Sol-II and sulphurized at different temperatures

were also studied and the refined bond angles were found to match with the reported values. The higher crystallite size was observed for the precursor film with thiourea further annealed in sulphur atmosphere but from SEM, grain size is found to be low. Elemental compositions of the films were studied by EDXS equipped with SEM. Cu-poor condition was observed, but Zn-rich condition was not observed. Hence the favourable Cu-poor and Zn-rich conditions were not observed in these two spray coating routes. The films deposited by both routes exhibited an optimum bandgap and higher optical absorption coefficients ($> 10^4$ $cm^{-1}$) in the visible region. In both the cases, bandgap of the films decreases with the increase in sulphurization temperature. Hall measurements indicated *p* type conductivity for all films. Carrier concentration, mobility and resistivity of the non-thiourea films sulphurized at 550 °C were found to be $1.544 \times 10^{19}$ $cm^{-3}$, 0.87 $cm^2V^{-1}$ $s^{-1}$ and 0.46 Ω·cm and for thiourea films sulphurized at 550 °C,

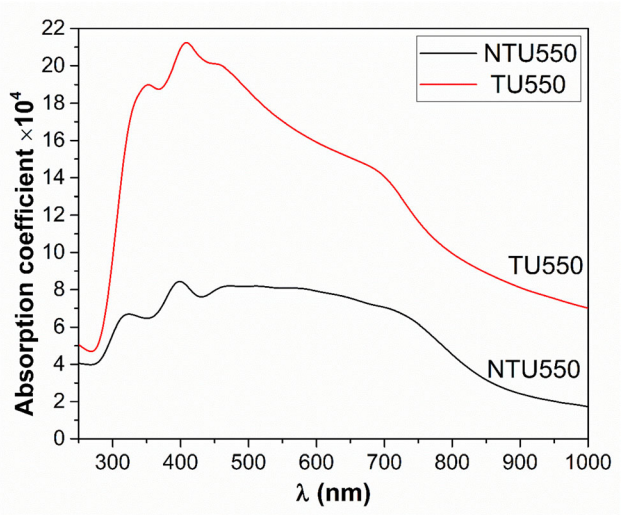


**Fig. 7** Absorption coefficient versus wavelength plots for NTU500 and TU500 films

the values obtained were $3.67 \times 10^{19}$ $cm^{-3}$, 0.33 $cm^2V^{-1}$ $s^{-1}$ and 0.52 Ω·cm, respectively. Carrier mobility was low for the CZTS films prepared and sulphurized from both the precursors. With the same parameters of spray coating, CZTS thin films prepared by suphurizing the precursor film with sulphur yielded maximum film thickness. Both the films show comparable properties, and the films coated with thiourea show the most promising results in terms of crystallite size, bandgap and absorption coefficients.

## Acknowledgements

Research Grant received from the Department of Science & Technology, Government of India (No. DST/TM/SERI /2K12/120) is gratefully acknowledged. The authors are thankful to the Director, C-MET, Thrissur for extending the facilities to carry out this work. We are also grateful to Dr. V. Raghavendra Reddy, UGC-DAE Consortium for Scientific Research, Indore for the grazing incidence X-ray diffraction measurements.

## Author contributions

PP: Investigation, Writing—Original draft preparation, Formal Analysis; VGS: Investigation; IPS: Resources, Data curation; SNP: Conceptualization, Supervision, Methodology, Writing—Reviewing and Editing. All authors read and approved the final manuscript.

## Funding

The research leading to these results received funding from the Department of Science & Technology, Government of India under Grant Agreement No. DST/TM/SERI /2K12/120.

## Compliance with ethical standards

**Conflict of interest** The authors have no conflicts of interest to declare that are relevant to the content of this article. The authors further declare that they have no known competing financial interests or personal relationships that could have appeared to influence the work reported in this paper.

**Ethical approval** The manuscript is original and has not been previously published, is not currently submitted for review to any other journal and will not be submitted elsewhere before a decision is made by Journal of Materials Science: Materials in Electronics.

## References

1. K. Pal, P. Singh, A. Bhaduri, K.B. Thapa, Sol. Energy Mater. Sol. Cells **196**, 138 (2019)
2. M.D. Wang, M.T. Winkler, O. Gunawan, T. Gokmen, T.K. Todorov, Y. Zhu, Adv. Energy Mater. **4**, 1301465 (2014)
3. V.G. Rajeshmon, C.S. Kartha, K.P. Vijayakumar, C. Sanjeeviraja, T. Abe, Y. Kashiwaba, Sol. Energy **85**, 249 (2011)
4. P. Prabeesh, I.P. Selvam, S.N. Potty, Thin Solid Films **606**, 94 (2016)
5. K. Tanaka, N. Moritake, H. Uchiki, Sol. Energy Mater. Sol. Cells **91**, 1199 (2007)
6. P. Prabeesh, K.V. Vysakh, I.P. Selvam, S.N. Potty, J. Electron. Mater. **47**, 5396 (2018)
7. P. Prabeesh, I.P. Selvam, S.N. Potty, Mater. Res. Express **6**, 065509 (2019)
8. K. Loan, P. Thi, D. Anh, T. Nguyen, H. Ke, T. Quynh, A. Le, J. Sol-Gel Sci. Technol. **83**, 324 (2017)
9. T.H. Nguyen, S. Fujikawa, T. Harada, J. Chantana, T. Minemoto, S. Nakanishi, S. Ikeda, Chemsuschem **9**, 2414 (2016)
10. N. Nakayama, K. Ito, Appl. Surf. Sci. **92**, 171 (1996)
11. M.Z. Ansari, N. Khare, Mater. Sci. Semicond. Process. **63**, 220 (2017)

12. M. Khammar, F. Ynineb, S. Guitouni, Y. Bouznit, N. Attaf, Appl. Phys. A Mater. Sci. Process. **126**, 1 (2020)
13. M.I. Fathima, A.M.S. Arulanantham, K.S.J. Wilson, Mater. Res. Express **7**, 015510 (2019)
14. K.V. Gunavathy, K. Tamilarasan, C. Rangasami, A.M.S. Arulanantham, Int. J. Energy Res. **44**, 7371 (2020)
15. K.V. Gunavathy, K. Tamilarasan, C. Rangasami, A.M.S. Arulanantham, Int. J. Energy Res. **43**, 7716 (2019)
16. R.J. Deokate, R.S. Kate, S.C. Bulakhe, J. Mater. Sci. Mater. Electron. **30**, 3530 (2019)
17. S. Lie, S.W. Leow, D.M. Bishop, M. Guc, V. Izquierdo-Roca, O. Gunawan, L.H. Wong, ACS Appl. Mater. Interfaces **11**, 25824 (2019)
18. S. Ahn, T.H. Son, A. Cho, J. Gwak, J.H. Yun, K. Shin, S.K. Ahn, S.H. Park, K. Yoon, Chemsuschem **5**, 1773 (2012)
19. P. Prabeesh, P. Saritha, I.P. Selvam, S.N. Potty, Mater. Res. Bull. **86**, 295 (2017)
20. T. Kunihiko, N. Moritake, H. Uchiki, Sol. Energy Mater. Sol. Cells **91**, 1199 (2007)
21. A.Y. Oral, E. Menşur, M.H. Aslan, E. Başaran, Mater. Chem. Phys. **83**, 140 (2004)
22. Y. Sun, Y. Zhang, H. Wang, M. Xie, K. Zong, H. Zheng, Y. Shu, J. Liu, H. Yan, M. Zhu, W. Lau, J. Mater. Chem. A **1**, 6880 (2013)
23. D.B. Mitzi, O. Gunawan, T.K. Todorov, K. Wang, S. Guha, Sol. Energy Mater. Sol. Cells **95**, 1421 (2011)
24. P. Prabeesh, I.P. Selvam, S.N. Potty, Appl. Phys. A **124**, 225 (2018)
25. P.A. Fernandes, P.M.P. Salomé, A.F. Cunha, J. Alloys Compd. **509**, 7600 (2011)
26. D. Dumcenco, Y. Huang, Opt. Mater. (Amst). **35**, 419 (2013)
27. X. Fontané, E. Saucedo, J.R. Morante, D.M. Berg, P.J. Dale, S. Siebentritt, Appl. Phys. Lett. **98**, 4 (2011)
28. P.A. Fernandes, P.M.P. Salomé, A.F. Cunha, Thin Solid Films **517**, 2519 (2009)
29. G. Gurieva, M. Guc, L.I. Bruk, V. Izquierdo-Roca, A. Pérez Rodríguez, S. Schorr, E. Arushanov, Phys. Status Solidi C **10**, 1082 (2013)
30. K. Tanaka, N. Moritake, M. Oonuki, H. Uchiki, Jpn. J. Appl. Phys. **47**, 598 (2008)
31. W.G. Nilsen, Phys. Rev. **182**, 838 (1969)
32. P. Prabeesh, P. Saritha, P. Selvam, S.N. Potty, Adv. Mater. Proc. **2**, 46 (2017)
33. B.H. Toby, J. Appl. Crystallogr. **34**, 210 (2001)
34. S. Schorr, H. Hans Joachim, M. Ovar, Eur. J. Miner. **19**, 65 (2007)
35. S. Schorr, Sol. Energy Mater. Sol. Cells **95**, 1482 (2011)
36. H. Nozaki, T. Fukano, S. Ohta, Y. Seno, H. Katagiri, K. Jimbo, J. Alloys Compds. **524**, 22 (2012)
37. P. Prabeesh, V.G. Sajeesh, I.P. Selvam, M.S.D. Bharati, G.M. Rao, S.N. Potty, Sol. Energy **207**, 419 (2020)
38. S. Chen, X.G. Gong, A. Walsh, S. Wei, Appl. Phys. Lett. **96**, 021902 (2010)
39. H. Guan, H. Shen, W. Wang, J. Mater. Sci. Mater. Electron. **28**, 14424 (2017)
40. S. Huang, W. Luo, Z. Zou, J. Phys. D. Appl. Phys. **46**, 235108 (2013)
41. M.A. Lloyd, D. Bishop, O. Gunawan, B. Mccandless, IEEE 43rd Photovolt. Spec. Conf. **2016**, 3636 (2016)
42. A. Redinger, D.M. Berg, P.J. Dale, S. Siebentritt, J. Am. Chem. Soc. **133**, 3320 (2011)
43. V.T. Tiong, J. Bell, H. Wang, Beilstein J. Nanotechnol. **5**, 438 (2014)
44. A.C. Lokhande, R.B.V. Chalapathy, M. He, E. Jo, M. Gang, S.A. Pawar, C.D. Lokhande, J.H. Kim, Sol. Energy Mater. Sol. Cells **153**, 84 (2016)
45. S. Siebentritt, Thin Solid Films **535**, 1 (2013)
46. B. Long, S. Cheng, Y. Lai, H. Zhou, J. Yu, Q. Zheng, Thin Solid Films **573**, 117 (2014)
47. J.J. Scragg, P.J. Dale, L.M. Peter, G. Zoppi, I. Forbes, Phys. Status Solidi Basic Res. **245**, 1772 (2008)
48. O.H. Tanaka, T. Nagatomo, D. Kawasaki, M. Nishio, Q. Guo, A. Wakahara, A. Yoshida, J. Phys. Chem. Solids **66**, 1978 (2005)
49. W. Xinkun, L. Wei, C. Shuying, L. Yunfeng, J. Semicond. **33**, 2010 (2012)
50. F. Liu, Y. Li, K. Zhang, B. Wang, C. Yan, Y. Lai, Z. Zhang, J. Li, Y. Liu, Sol. Energy Mater. Sol. Cells **94**, 2431 (2010)